Computational study of neuronal networks with spatial constraints by means of the Izhikevich model

Author: Guillem Güell Paule
*Facultat de Física, Universitat de Barcelona, Diagonal 645, 08028 Barcelona, Spain.**

Advisor: Jordi Soriano Fradera

Abstract: A huge effort has been made along the last 20 years to map the detailed structural organisation of neural networks. The main reason behind this effort is to understand the relationship between the structure of the network and its dynamics or functional traits. To advance in this quest, numerical simulations have emerged to help exploring the relation between structure and function. Here we used the Izhikevich model to simulate neuronal networks with spatial constraints. We launched numerical simulations of 1000 neurons in two different modular networks, and mimicking designs reported in experiments. We observed that some information about structure can be glimpsed when the spatial constraints are very strong. In general, however, the properties of the underlying structural network differ greatly from those obtained from the simulations, indicating that the assessment of structural connectivity from just dynamics is not possible. We also applied damage to the networks, and observed that targeted attacks strongly affects the activity and functional traits of the networks under study.

I. INTRODUCTION

The brain is arguably one of the ultimate elements of complexity and, although it has been the subject of study since the dawn of civilisation, it was not until the second half of the 20th century that the term 'neuroscience' was introduced into scientific fields. Although this discipline has been approached from very different points of view, such as the social or biological sciences, the ultimate study of the brain involves treating it as a complex system. Neurons, together with glia cells, are the fundamental units of the nervous system and therefore of the brain. The first mathematical model, introduced in 1952 by Hodgkin and Huxley (HH) [1] and subsequent modifications of this model revealed that neurons must be treated as non–linear units that interact to one another, leading to non–trivial emergent behaviour that extends along different spatiotemporal scales.

The large size of the human brain makes it very difficult to study at the structural level of micro–connectomics, *i.e.* connectivity at the level of synapses between neurons. This is why the study of neural networks through *in vitro* cultures has become one of the most widely used tools in neuroscience. These cultures, usually build at mesoscopic scales (from micrometres to several millimetres), allow a wide variety of complex phenomena to be explored. In turn, cultures can be considered as the circuits that make up the different areas of the human brain on a macroscopic scale.

In neuronal cultures, and just as in real neural networks, neurons are not necessarily arranged in an organised crystal–like structure. Indeed, using modern neuroengineering technologies, neurons can be placed in predefined locations and connections accurately dictated to shape complex networks that mimic the topological traits of the brain or its complex dynamics.

A simple way to place neurons or connections in specific places is by implementing strong spatial constraints, that is, by placing the neurons in physical traps (valleys or crevices in a substrate) that typically favour a strong local connectivity while reducing the capacity of neurons to connect with far away neighbours. This topology allows for the occurrence of balanced local–global dynamics, in which synchronisation periods (*network bursts*) at the system scale combine with activations in groups at a local level. Altogether, this balance enables information transfer at the global level in combination with specialised information processing at the local level [2].

Although neuronal cultures are an excellent tool for experimental neuroscience, the design of adequate spatial constraints is difficult. To help experimentalists to observe a variety of dynamic phenomena as rich as possible, computational neuroscience has brought to light simple yet powerful resources in which the impact of spatial constraints can be explored at will.

Indeed, the dynamics between neurons can be easily simulated on complex network using the Izhikevich's model [3]. Conceptually, one can establish a complex network of synaptic connections among neurons (*structural connectivity*) and then incorporate dynamics. Next, one can extract the *functional connectivity* between neurons from the analysis of the dynamics, and explore whether the functional connectivity approaches the structural connectivity and under which conditions their similarity is the closest. Actually, the relationship between functional and structural connectivity is one of the big open questions in neuroscience, and simulations help exploring it. For instance, that two neurons fire together does not imply that they are directly connected, and possibly their synchronous dynamics is mediated by a third neuron. What simulations offer is to explore small changes in

* gguellpa20@alumnes.ub.edu

the structure of networks to investigate changes in their functionality.

In this Thesis we explored suing numerical simulations the impact of spatial constraints. Inspired by recent experiments [4],[5],[6], we placed neurons in small islands or along parallel stripes. We investigated the resulting dynamics in the studied networks and explored the emergence of complex dynamics as well as the relationship between structural and functional connectivity. We observed that structural and functional networks were similar only when the spatial constraints were very strong, *i.e.* when the physical connectivity strongly dictated the dynamics of the emerging network.

II. METHODS

In this work, neurons are placed in two types of geometries:

- **Aggregated construction:** Neurons are arranged in small isolated islands (called 'modules') embedded in a two–dimensional Euclidean space, FIG. 1. Progressively, a percentage of the internal connections of the modules is rewired to form long–distance connections between neurons in different modules. Thus, a percentage of rewiring is found that leads to a balance between local and global behaviour in the system.
- **Regular patterning construction:** Neurons are arranged in a striped pattern embedded in a quasi two-dimensional Euclidean space. In this pattern the neurons can be on two levels of different heights, FIG. 2. These heights introduce a bias, as neurons in the top stripes connect more easily with neurons in the bottom stripes than vice versa. The number of stripes a neuron in a given stripe is allowed to access can be progressively changed, as well as the height difference between stripes.

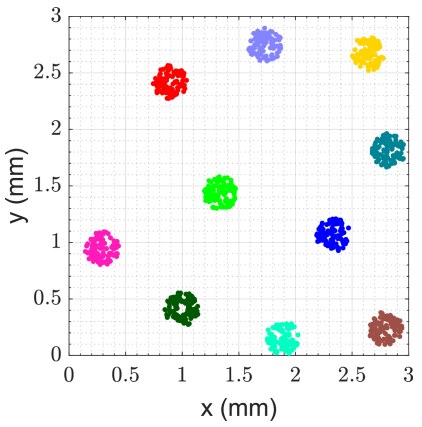

FIG. 1. Positions of neurons in the aggregated network. Each colour refers to a different community.

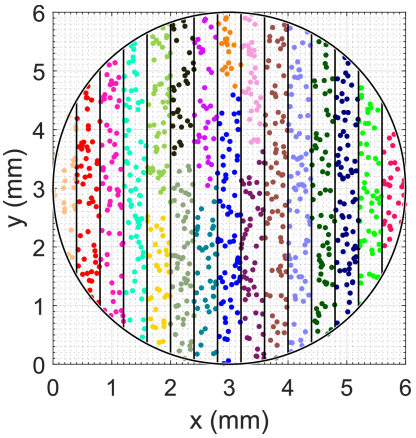

FIG. 2. Positions of neurons in the striped network. Each colour refers to a different community.

Both in *in vitro* cultures and in the brain itself neurons and connections die, either in reduced fractions due to ageing or in large fractions, due to neurodegenerative diseases such as Parkinson's or Alzheimer's disease. For this reason, we also explored in the present Thesis the deletion of nodes and their impact in collective dynamics. In the simulations, damaging a neuron means eliminating all interactions between it and those with which it had a structural connection.

A. Spatial network

For the two geometries introduced above, the *in-silico* networks have a total of $N = 1000$ cortical neurons, of which 80% corresponds to excitatory neurons (N_e) and 20% to inhibitory neurons (N_i). These are the typical fractions in the brain and proportionate a good ratio of positive and negative inputs so as to reach *quorum* for the neurons to fire.

The aggregated neurons shape highly compact modules that are laid on a 3×3 mm^2 grid. The aggregates have a radius of $r = 0.15$ mm but act as hard disks with exclusion radius $r^* = 2r$. In each of the 10 modules there are 80% N_e and 20% N_i.

The neurons on the striped pattern lay on a 6×6 mm^2 grid, but are located only in the inscribed circle of radius $r = 3$ mm. To model the effective height of the two–level pattern of the bands we introduce two variables, $h_\uparrow$ and $h_\downarrow$ which are the probabilities that have neurons from lower (higher) bands to connect to others at higher (lower) bands.

Once that the neurons have been placed uniformly inside the circles in both geometries, we store the connections of the structural network in the matrix $S = \{s_{ij}\}$. As the network is directed, this matrix will be asymmetric. The in–going connections, that is, connections from neuron j to neuron i are stored in columns and out–going connections are stored in rows. We construct S as fol-

lows:

First, we compute all the Euclidean distances between pairs of neurons and we store them in the symmetric matrix $\mathcal{D} = \{d_{ij}\}$. We then calculate the interaction probability, which decays linearly with the distance between neurons,

$$P(d_{ij}) \equiv p_{ij} = -\frac{d_{ij}}{d_{max}} + 1, \tag{1}$$

such that $P(d_{ij} = 0) = 1$ and $P(d_{ij} = d_{\max}) = 0$, where $d_{\max}$ is the maximum allowed length of an axon. In the case of discs, $d_{\max} = 2r$ and in the case of the striped pattern $d_{\max} = 1$ mm. Next, a matrix $X = \{x_{ij}\}$ is generated, the elements of which are random numbers $U(0, 1)$, which is compared with the probabilities of the elements in the matrix $\mathcal{D}$ by constructing the binary matrix S with ones in the elements for $x_{ij} < p_{ij}$ and zeros in the elements for $x_{ij} > p_{ij}$. Finally, the columns corresponding to inhibitory neurons are given a negative weight.

In practice, there are also long-distance connections between neurons. To create them, a rewiring is done between neurons, randomly choosing a fixed percentage of connections that are eliminated to be formed with others, always avoiding self and multiple connections. In the case of the aggregated network where we have a strong intra-connection, the rewiring results in the formation of long-distance connections, linking the different modules.

We note that, for correctly implementing neuronal dynamics, neurons require a certain strength in the connections. Thus, S is used as a weighted network during the simulations. However, S is considered as unweighted (binnarized) for calculating the various network properties described in II C. Thus, it can be ensured that these properties reflect network key structure rather than weights.

B. Dynamical model

As mentioned above, neurons are, together with glia, the fundamental units of the nervous system. Through them we are able to perceive and process information from the world around us. Although not all neurons are by no means the same, nor do they all have the same functions, a model neuron can be considered to receive input from other neurons via the dendrites, integrate it and conduct it through the axon to other neurons. The main element that mediates the transmission of pulses between the sending (presynaptic) and receiving (postsynaptic) neuron is the membrane of the latter. The membrane potential is at rest at about -65 mV. When the postsynaptic neuron receives an input from an excitatory (inhibitory) neuron there is a net flow of ions such that the potential gets increased (decreased). These potentials are called excitatory (inhibitory) postsynaptic potentials, EPSP and IPSP, respectively. If the sum of the positive and negative contributions surpass a threshold (typically of about -55 mV) in a short period of time (of the order of some milliseconds) there is *quorum*. This results in a huge fast depolarization of the membrane, reaching 30 mV, followed by a fast repolarization, what is called an action potential (AP) and it is said that the neuron has fired and there is a spike, sending the input to further neurons.

As introduced above, Hodgkin and Huxley provided the first formal mathematical description of the AP by studying the electrical properties of the giant axon of the squid. The resulting model involved several nonlinear coupled differential equations not solvable at the moment. Several years later, FitzHugh and Nagumo (FHN) simplified the model, showing that only two dynamical variables are required, one for the membrane potential, v, and one for the recovery of the membrane, u. This model can be analysed with the tools provided in dynamical systems theory (nullclines, equilibrium points,...) and provided a good description of excitable systems. It was not until 2003 that Izhikevich presented a highly fast and efficient computational model and at the same time very plausible from a biological point of view. One of the most remarkable differences between this model with respect to the previous HH and FHN models is that a quadratic dependence on v is sufficient to account for its non–linear behaviour. As already stated, this model is the one used in this project under some modifications, and is described as follows.

The main equations read

$$\frac{dv}{dt} = C_1 v^2 + C_2 v + C_3 - u + I + \eta, \tag{2}$$

$$\frac{du}{dt} = a\,(bv - u)\,, \tag{3}$$

such that variables u and v recover after an occurrence of an spike:

$$\text{if } v \geq 30 \text{ mV}, \begin{cases} v \leftarrow c, \\ u \leftarrow u + d. \end{cases} \tag{4}$$

To solve this differential equations in simulations we use the Euler method with a time step of 1 ms.

In addition to the already mentioned variables u and v, C_1, C_2 and C_3 are constants, I accounts for the received synaptic currents, η correspond to the random thalamic inputs *i.e.* noise, and a, b, c and d are parameters that can be tuned to get different modes and characteristics of neurons. The parameters a and b describe the time scale and the sensitivity of of recovery of the variable u, respectively, and the parameters c and d account for the after–spike reset values of variables v and u.

By varying some of the parameters used in Izhikevich's original paper [3] we can obtain different dynamics.

On the one hand, the time–scale obtained with Izhikevich's default code does not match with the one observed in typical experiments, in which neurons coactivate together in a quasi–synchronous manner (*network bursts*

every few seconds. Thus, in our simulations, we seek to get inter–burst intervals (IBIs) between 5 and 10 seconds instead of getting of the order of 5 spikes per second. This adjustment in time scales is obtained by adding an extra variable to the model, the *short–term postsynaptic depression*. In real systems, neurons need neurotransmitters for the signal to pass from one neuron to another. If there is the case that one neuron gets too many inputs in a short period of time, neurotransmitters get depleted from presynaptic vesicles and some characteristic time τ_D is needed to recover part of them.

On the other hand, by tuning parameters $a - d$ we can change the shape and frequency of the AP trains. Originally, values were chosen to have an heterogeneity of neurons, biased towards a regular spiking (RS) and towards fast spiking (FS) excitatory and inhibitory neurons, respectively. The problem with having FS–type inhibitory neurons is that once we have introduced the long timescale of depression they get sort of decoupled of the rest of the dynamics and they fire at a very high frequency. This introduces an artefact when analysing the obtained spikes. Introduced in [7], one way to deal with this is to use the same values of a, b, c and d for both excitatory and inhibitory neurons, so that the latter acts more like the excitatory ones but still having negative weights in the adjacency matrix S.

The synaptic current of neuron j at time t, $I_j(t)$ is the contribution of currents induced from all the neurons i that connect to j and fire at the same time $t = t_m$:

$$I_j(t) = \sum_{i=1}^{k_{in}^j} g_{ij} \sum_{t_m<t} D_j(t)\delta(t - t_m). \tag{5}$$

Neurons are said to be pulse–coupled, as a substantial amount of them has to fire at the same instant to reach *quorum*. Other models relax this condition, allowing the postsynaptic membrane potential to decay exponentially with a characteristic time τ_A, facilitating synchronisation.

In Eq. (5) $g_{ij} \equiv g_A$ is the strength of the synapses, *i.e.* the values in the weighted adjacency matrix S. $D_i(t) \equiv D$ is the variable that accounts for the synaptic depression. This variable has a rest value of 1 until neuron i fires and its value is reduced to βD, with $\beta < 1$. As stated before, τ_D is the characteristic time that needs D to decay towards 1. The governing equation of synaptic depression reads

$$\frac{dD_j(t)}{dt} = \frac{1}{\tau_D}(1 - D) - (1 - \beta)D\delta(t - t_m). \tag{6}$$

The values of the parameters of the model are presented in TABLE. I.

TABLE I. Values of the parameters in the simulations.

Model parameters	
Recovery scale of u	$a = 0.02$ ms^{-1}
Sensitivity of v	$b = 0.2$
After-spike reset value of v	$c = (-65, -50)$ mV
After-spike reset value of u	$d = (2, 8)$ mV
Constants	$C_1 = 0.04$ mV^{-1}ms^{-1}
	$C_2 = 5$ ms^{-1}
	$C_3 = 140$ mV ms^{-1}
Thalamic input	$\eta \in N(0, 2.6)$ mVs^{-1}
Synapse strength (modules)	$g_A = 6.5$ mV ms^{-1}
Synapse strength (stripes)	g_A=9 mV ms^{-1}
Synaptic depression recovery time	$\tau_D = 3000$ ms
Synaptic depression decay	$\beta = 0.7$

C. Network properties

As stated above, the neurons in cultures form connections leading to a directed network. From graph theory many measures can be computed to extract properties and features of the resulting network. Since we only use excitatory neurons for the calculation of functional connectivity, the various quantities described below are calculated from neurons of this type.

- **Correlation length**, δ. This is computed as the relative ratio between the average axonal length, a_L, and the characteristic system size, L,

$$\delta = a_L/L, \tag{7}$$

  where $L = 2\sqrt{A/\pi}$ such that A is the characteristic area of the network. a_L is computed by taking average values of the non–zero elements of the matrix resulting from the element–wise multiplication (Hadamard product) of the matrix of the positions and the matrix of connections, $\langle S \circ D \rangle$.

  In the case of the aggregated network the area of the grid is $A = 9$ mm^2 and a_L depends in both the connections inside the modules and the ones between modules as a result of the rewiring. In the case of the striped network $A = \pi r^2 = 9\pi$ mm^2 is equal to the area of the inscribed circle and a_L depends on the maximum number of stripes that can explore a neuron from a given band and on the effective height of the stripes, that is, on the parameters $h_\uparrow$ and $h_\downarrow$. These are used to regulate the probability of connection between neurons in contiguous bands. The probability is decreased by a factor $h_\uparrow$ when a neuron in a lower band wants to connect to a neuron in a higher band, and the probability is decreased by a factor $h_\downarrow$ in the opposite case. These parameters take values in the interval $[0, 1]$ such that a value of 0 is equivalent to an infinite effective height and a value of 1 to a zero effective height.

- **Gini coefficient**, $\Lambda \in [0, 1]$. This coefficient is a measure of the aggregation of the physical underlying network. To compute this number we first overlay the network on a grid with unit cells of size $s = 10^{-2}$ mm^2 and we count the neurons in each of

these cells. Then we order the counts from the lowest to the highest value and we plot the cumulative fraction of neurons with respect to the cumulative fraction of area occupied by them. $\Lambda/2$ is the area under the (Lorenz) curve that deviates from the totally homogeneous case. Thus, $\Lambda = 0$ corresponds to a grid–like network and $\Lambda \simeq 1$ to the case we had all the neurons in one of the cells (spatial homogeneous distribution of neurons).

In the case of the modular network the grid spans the 3×3 mm^2 area whereas in the case of the striped network we discount a number of cells proportional to the area between the circle and the 6×6 mm^2 square.

- **Node degree**, k, and degree distribution. As the network is directed the degree of the node j is computed as the sum of the number of in–going and out–going connections with other neurons, $k^j = k^j_{in} + k^j_{out}$. The degree distribution, $P(k)$ is the probability density function (PDF) of having a node with degree k. Similarly, the number of times we have a node of degree k is calculated by means of a histogram.

The following magnitudes are computed using the *Brain Connectivity Toolbox* in MATLAB.

- **Modularity**, $Q \in [0, 1]$. This magnitude quantifies how likely is that a neuron belongs to a community, that is, that the number of neuronal connections within the community is higher than between communities. A high value of Q is expected for very modular networks.

  The directed version of the modularity proposed by Newman [8] reads

$$Q = \sum_{i,j} \left[\frac{S_{ij}}{m} - \frac{k^i_{out} k^j_{in}}{m^2} \right] \delta\left(c_i, c_j\right), \tag{8}$$

  where m is the number of edges and $k^i_{out}k^j_{in}$ is the probability of having a link that goes from neuron i to neuron j. The value of Q is maximised using the iterative Louvain Method. The result also gives the number of communities NC. Each of them is a sharp sub-network of the original one, as every neuron can belong to only one community.

- **Global efficiency**, $G_{\text{eff}} \in [0, 1]$. It quantifies how complete is a network, by making an average of the inverse of the shortest (topological) path length, σ_{ij} between pairs of nodes i and j. G_{eff} is a direct measure of how easily is to exchange information across the network, *i.e.*, the global integration in the network. For binary unweighted graphs this magnitude reads

$$G_{\text{eff}} = \frac{1}{N(N-1)} \sum_{0\leq i,j\leq N} \frac{1}{\sigma_{ij}}. \tag{9}$$

  We expect to find a value close to 0 for networks in which almost all the nodes are unconnected and a value near 1 for almost fully–connected graphs.

- **Local efficiency**, $L_{\text{eff}} \in [0, 1]$. It quantifies how ease is to exchange information at a local level. L_{eff} is computed as the average of the global efficiencies computed in each of the nodes, only between their nearest neighbours,

$$L_{\text{eff}} = \frac{1}{N} \sum_i G_{\text{eff}}(nn_i). \tag{10}$$

  Here nn_i indicates the nearest neighbours of node i.

- **Betweenness centrality**, BC. Quantifies the importance of a node. BC(i) is the sum of the fractions of (topological) shortest paths that go through node i linking pairs of nodes $j - k$, $\sigma_{jk}(i)$, with respect to the total number of (topological) shortest paths between nodes j and k, σ_{jk}.

$$\text{BC}(i) = \sum_{j,k} \frac{\sigma_{jk}(i)}{\sigma_{jk}}. \tag{11}$$

D. Calcium dynamics

One of the most used techniques in the laboratory to record activity of firing neurons is calcium imaging. The processes related to vesicle release in neurotransmitter transport are mediated by Ca^{2+}, such that the concentration of calcium in the intracellular medium increases by a factor of 10^3 in each firing. This increase can be captured by a calcium fluorescence indicator by means of the green fluorescence protein (GFP). This is a protein that in the presence of calcium alters its conformation and becomes fluorescent. When this happens, if the culture is irradiated with blue light, the GFP is excited and re–emits the light in green, making possible to observe which neurons fire and which do not. The major drawback is that the time it takes for the calcium ions to bind to the GFP mask the action potential structure.

Although the calcium signal is usually used to infer the firing trains here we do the reverse conversion to obtain the calcium signal that would allow us to compare with the one obtained in the experiments. This conversion is done using the model proposed by Vogelstein et al. [9], described as follows.

Each action potential caused by a neuron at time t results in a calcium concentration of

$$\left[Ca^{2+}\right]_t = \left[Ca^{2+}\right]_{t-1} \left(1 - \frac{\delta t}{\tau_{Ca}}\right) + A_{Ca} n_t, \tag{12}$$

where $\delta t = 1$ ms is the time-step of the simulations, τ_{Ca} is the characteristic decaying time of the calcium concentration, $A_{Ca} = 50$ μM is the instantaneously jump in concentration after each spike and n_t the number of action potentials at time t.

E. Simulating damage in the networks

By introducing some substances to the real biological networks it is possible to block neurotransmitters, receptors or even the voltage–gated channels, what clearly affect the dynamics of the system. Here we are interested in considering the deletion of some neurons to check how this affects to both structural and functional results, in a similar way as in [10].

Complex networks have the small–world property, which means that networks are very compact so that each node is very close (topologically) to any other, resulting in a structure robust to random attacks. Thus, what we do here is to do targeted attacks at the most important nodes in the network. In particular, we look for the nodes with highest degree (hubs) and for those with highest betweenness coefficient to delete the top 5% nodes in each of the last two classes.

F. Functional connectivity analysis

The simulations of the designed structural networks in the context of the Izhikevich model provides trains of activity for each neuron. These data (*raster plot*) can be analyzed to extract the functional connectivity of the network, which concpetually captures the exchange of information among active neurons.

Different approaches can be used to analyse the data obtained from the raster plots and draw the functional networks. The simplest method is to use cross-correlation (XC), *i.e.*, to calculate Pearson's coefficients, which measure the linear correlation of two signals to quantify their similarity. Although good for inferring the level of synchronisation, XC does not give us information on directionality, *i.e.*, causality. In addition, data in neuroscience tends to correlate easily, making XC susceptible to artefacts.

A more robust approach is to calculate the Mutual Information (MI) between signals. This estimates the mutual dependence between two signals using information theory concepts. Although it is a non–linear measure it also does not provide causality between signals.

A generalisation of the concept of information transfer is Transfer Entropy (TE). It measures the amount of information directed from a signal Y to a signal X by calculating the decrease in uncertainty in X knowing the past values of signals Y and X. Even knowing the amount of bits exchanged, it does not provide a value for the strength of the interactions and the results obtained are usually difficult to interpret. However, those neurons that transfer more information are more likely to have causal interactions. The data procured by TE is standardised, such that

$$z = \frac{TE_{Y\to X} - \langle TE\rangle}{\sigma_{TE}}, \tag{13}$$

where $\langle TE\rangle$ and σ are the mean value and standard deviation of the data, respectively. z is known as the z-score and indicates the threshold in standard deviation units from where one can accept the data as significant. With $z = 0.5$ almost all the data is taken while $z = 3$ the largest transfers of entropy are taken, allowing to identify the neurons that influence the others the most.

III. RESULTS

A. Overview of typical simulations and impact of aggregation

To start with, we provide in FIG. 3 typical simulations, where we can see the strong spatial embedding of the aggregated network and the more relaxed one for the stripes one. The raster plot shows that activity is rich and neurons in the aggregates or stripes tend to activate together very strongly, indicating they are quite isolated, unlike what we would expect from a uniform network where all the neurons tend to synchronise.

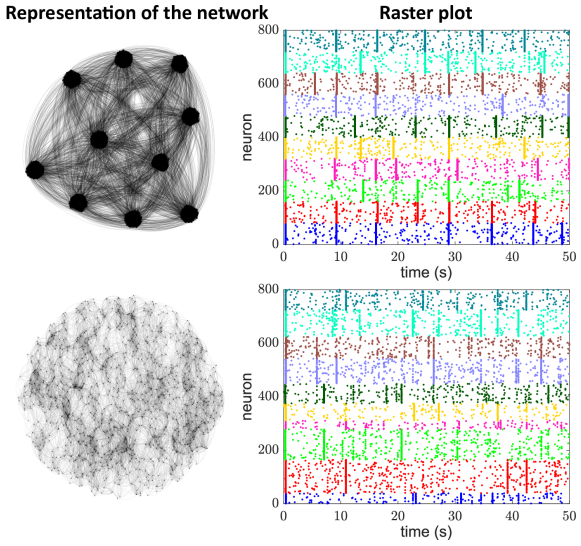

FIG. 3. Representation of the aggregated and striped networks and activity of the neurons shown in the raster plot.

As presented in Methods, the Gini coefficient measures the aggregation of neurons in the network based on their positions. As these are fixed for all simulations, Λ will be constant. In the case of the disc–like aggregates we obtain a value $\Lambda = 0.92$, while we obtain $\Lambda = 0.74$ for the striped pattern. These results reflect what could have been anticipated just by looking at FIGs. 1 and 2. Aggregation is substantial in the case of the aggregated network, where Λ is close to 1, and weaker in the case of the striped network. The Lorenz curve obtained for both geometries is presented in FIG. 4.

To be sure that we had strong spatial constraints in the networks, we calculated the correlation length δ, also

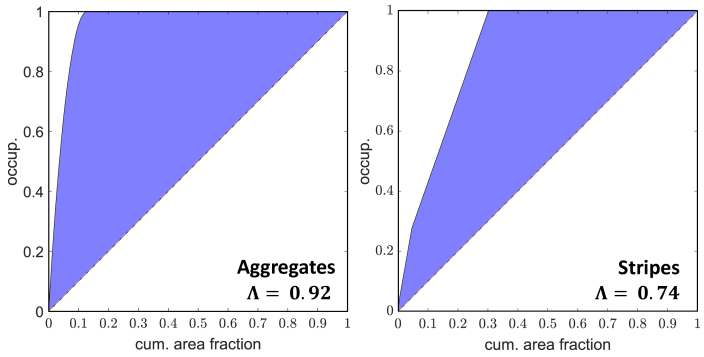

FIG. 4. Representation of the aggregation via the Lorenz curve for the aggregated network (left) and for the striped network (right).

defined in the methods section. δ depends on the connections between neurons and will therefore vary when changing the parameters that regulate the connectivity. A value $\delta \ll 1$ indicates that the axon length is negligible compared to the characteristic length of the network and the spatial restrictions are relevant. Conversely, for $\delta \gg 1$ the constraints on the space in which the lattice is located are negligible. The values for δ are shown, as well as the rest of the computed magnitudes computed in the structural networks, in Tables. II and III.

TABLE II. For each of the simulations done in the aggregated network, for different rewiring values and damage to nodes with a centrality coefficient and with a higher degree, the following magnitudes are shown: average axon length, correlation length, average network degree, modularity, global and local efficiencies. Values calculated for the structural connectivity network.

# Simulation	1	2	3	4	5	6
Rewiring (%)	0	4	6.5	13	20	6.5
Damage BC (%)	-	-	-	-	-	5
Damage k (%)	-	-	-	-	-	5
a_L (mm)	0.11	0.17	0.21	0.32	0.42	0.21
δ	0.03	0.05	0.06	0.09	0.12	0.06
$\langle k \rangle$	86	86	86	86	86	79
Q	0.90	0.86	0.84	0.77	0.71	0.84
G_{eff}	0.08	0.40	0.42	0.45	0.46	0.41
L_{eff}	0.91	0.85	0.82	0.77	0.74	0.81

B. Impact of spatial embedding and rewiring on aggregated networks

In the case of aggregates, we tune the percentage of applied rewiring with respect to the case in which the modules are isolated (this being 0% of rewiring) up to a maximum of 20%.

For all simulations, and by looking at Table II, we see that the value of a_L is small. Comparing with the characteristic length of the system, we see that we get $\delta \simeq 0.07$ on average, which implies a strong spatial constraint. For the case of the fully isolated aggregates (simulation #1) we observe a large modularity ($Q = 0.90$), which was to be expected given the highly–compact spatial arrangement of the neurons. This indicates that the information can be processed very well at the local level, obtaining a value of L_{eff} very close to 1, but impossible to transmit at the global level, being G_{eff} almost zero. This reflects that many of the pairs of nodes to be chosen have an infinite topological distance between them.

It is observed that, as the rewiring percentage increases, so does a_L. This is consistent, since the rewiring is of long distance, *i.e.*, that for a fixed rewiring ratio a number of connections within the same aggregate will be chosen randomly to connect neurons that most likely are in different aggregates. Thus, δ also increases, although even for 20% rewiring a very small correlation length is obtained.

As the different aggregates become more connected, the value of modularity decreases, although for the cases studied Q remains very large. This reflects the importance of the large number of connections between the neurons inside the different aggregates, which supports the inherent modular structure. This is also reflected in the local efficiency, since the minimum value, corresponding to the simulation with 20% rewiring, is still high ($L_{\text{eff}} = 0.74$). On the other hand, the global efficiency increases. Let us note that this magnitude increases very fast when the first long distance connections are formed; G_{eff} increases by a factor of 5 when going from independent modules to 4% rewiring, to then increasing steadily. The maximum value $G_{\text{eff}} = 0.46$ is sufficient to observe synchronous system behaviour. Therefore, if we are looking for a balance between local and global behaviour we have to stay with a percentage of rewiring between 0% and 20%. A percentage higher than 20% would destroy the inherent aggregate structure. The same would happen for a complete randomisation of the network. Thus, this indicates that a rewiring of 20% is a good reference for a non–spatial network. As seen in the raster plot in FIG. 8h, 6.5% rewiring is sufficient to achieve the balance of local–global behaviour.

C. Impact of spatial embedding and rewiring on the stripes' networks

In the case of the striped network we can regulate two parameters to study their implications for the network.

Firstly, we quantify the effective height of the stripes through the parameters $h_\uparrow$ and $h_\downarrow$ described earlier. Note that we speak of effective heights experienced by neurons in both low and high stripes, because although it is easier to connect from high to low stripes, neurons in high stripes prefer to connect with others at the same stripe than to form an axon towards a lower level. For this reason in the present study $h_\uparrow = 0.1$ and $h_\downarrow = 0.5$ are set, strongly disfavouring the formation of axons from low to

high stripes. We compare this condition with the homogeneous case (absence of stripes, $h_\uparrow = h_\downarrow = 1$) and with the case where $h_\uparrow = h_\downarrow = 0.35$, in which no distinction is made between low or high stripes as they all see the same effective height.

And, secondly, we can modify the number of adjacent stripes, n_{adj}. This regulates the number of stripes on the right and left to which a neuron in a given stripe can form connections. For such a construction, the maximum axonal length in absence of rewiring is $d_{\max} = 1$ mm. This parameter can be viewed of as introducing a bias, further favouring connection in the longitudinal direction (along stripes) over the transverse (across stripes).

TABLE III. For each of the simulations done in the striped network, for different rewiring values, number of adjacency stripes, effective heights and damage to nodes with a centrality coefficient and with a higher degree, the following magnitudes are shown: average axon length, correlation length, average network degree, modularity, global and local efficiencies. Values calculated for the structural connectivity network.

# Simulation	1	2	3	4	5	6	7
Rewiring (%)	0	0	0	0	0	0	10
n_{adj}	2	0	1	2	2	2	2
$h_\uparrow$	1	-	0.1	0.1	0.35	0.1	0.1
$h_\downarrow$	1	-	0.5	0.5	0.35	0.5	0.5
Damage BC (%)	-	-	-	-	-	5	-
Damage k (%)	-	-	-	-	-	5	-
a_L (mm)	0.49	0.37	0.41	0.42	0.43	0.41	0.60
δ	0.08	0.06	0.07	0.07	0.07	0.07	0.10
$\langle k \rangle$	53.3	19.2	27.1	27.4	29.2	23.8	27.4
Q	0.66	0.93	0.75	0.74	0.72	0.75	0.66
G_{eff}	0.30	0.03	0.21	0.22	0.24	0.21	0.32
L_{eff}	0.86	0.89	0.77	0.76	0.80	0.74	0.60

Given the arrangement of the neurons, we consider the homogeneous case (simulation #1) as the control model, since it is equivalent to the network obtained in the absence of stripes.

The most spatially constrained case is simulation #2 in which neurons only connect to their neighbours in the same stripe. This condition is equivalent to $h_\uparrow = h_\downarrow = 0$. Although a_L takes the smallest value in this simulation, this magnitude is small for all the other networks given the different parameters. Only in the case where we allow 10% rewiring we get a slightly larger value. However, $a_L \ll L$ and therefore $\delta \ll 1$.

The comparison of values for simulations with different numbers of adjacent stripes (#1 to #4) reveals that the substantial change in magnitudes is between $n_{\text{adj}} = 0$ and $n_{\text{adj}} = 1$, where Q and L_{eff} decrease but G_{eff} increases by a factor 7. From #2 to #4 more and more connections are formed and therefore $\langle k \rangle$ increases. a_L also increases but in this network, this magnitude has more dependence on the axonal length of the newly formed connections.

The comparison between the simulations for different values of $h_\uparrow$ and $h_\downarrow$ (#4 to #5) does not reveal major changes in the structural properties of both networks, although G_{eff} and L_{eff} are slightly larger in the case of simulation #5. What does change is the dynamics, as discussed later.

Note that for the case where we leave 10% rewiring (#7) we obtain, among all the simulations, the most efficient network globally but at the same time the least efficient network locally.

D. Comparison of structural and functional connectivity on aggregated and striped networks

As described in Methods, one has to carefully choose how to analyse the dynamic information obtained from the simulations, in this case the raster plots, to compute the effective or functional connectivity. Figure FIG. 5 and FIG. 6 show the comparison of XC and MI approaches for simulation #3 of aggregated network and #5 of the striped network, respectively. These simulations have been chosen as they correspond to the cases where the rewiring and the height of the stripes allow a balanced behaviour between local and global connectivity. As we can see in the figures, XC and MI are similar, but XC has many weak connections outside the diagonal that are not present in MI. Thus, the latter approach provides cleaner networks.

By using these MI results, we then adjusted the z–score in the TE approach to get matrices as similar as possible to MI. The idea is to get finally adjacency matrices that are directed but that are overall consistent with MI. During TE analysis, we considered z–score values of $z = \{0.5, 1, 2, 3\}$, and observed that the adjacency matrix most similar to MI was the one corresponding to $z = 1$. Thus, from here onwards, we took TE adjacency matrices with $z = 1$.

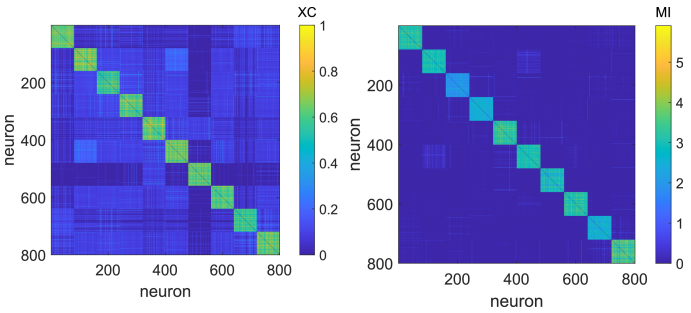

FIG. 5. XC (left) and MI (right) adjacency matrices from simulation #3 of the aggregated network.

With the TE effective connectivity in mind as the best connectivity inference approach, we proceeded to compare the structural and effective matrices. These matrices are shown in detail later in FIGs. 8 and 9. The idea here, however, was just to calculate the percentages of coincidence and error with respect to the structural matrix. The results, for different z–scores, are displayed in TABLE. IV.

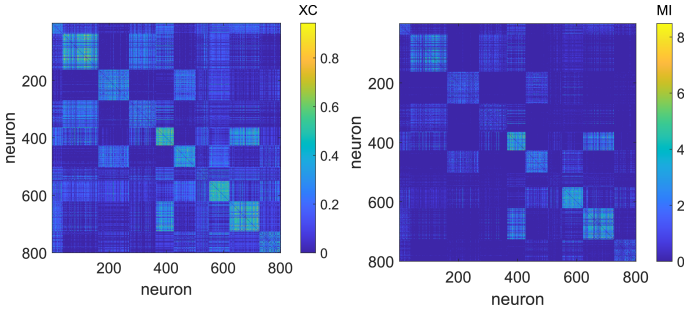

FIG. 6. XC (left) and MI (right) adjacency matrices from simulation #5 of the striped network.

TABLE IV. Values of the percentages of coincidence and error for different values of the z-score, for the simulations #3 of the aggregated network and #5 of the striped network.

Simulation	#3 (aggregates)				#5 (stripes)			
z-score	0.5	1	2	3	0.5	1	2	3
% coincidence	86.3	77.2	55.0	26.0	79.2	64.0	37.2	18.8
% error	9.9	5.4	3.0	1.3	21.1	11.4	3.4	1.0

We see how the error percentages are very low for $z = 3$, indicating that strong effective connections are also present in the structure. However, these are only 26% of all connections in the aggregated configuration and about 19% in the stripes configuration. We note that in simulation #3 the choice $z = 1$ implies more success and at the same time less error than for simulation #5, but for simplicity $z = 1$ is chosen systematically for all simulations.

The network properties calculated for the structural network can also be calculated for the effective networks. Results are presented in TABLE. V and TABLE. VI for each of the two networks studied.

TABLE V. Network properties computed from the effective connectivity obtained in the different simulations performed in the aggregated network.

# Simulation	1	2	3	4	5	6
Rewiring (%)	0	4	6.5	13	20	6.5
Damage BC (%)	-	-	-	-	-	5
Damage k (%)	-	-	-	-	-	5
a_L (mm)	0.21	0.47	0.35	0.85	1.08	0.49
δ	0.06	0.14	0.10	0.25	0.32	0.14
$\langle k \rangle$	152	159	148	215	221	154
Q	0.85	0.77	0.77	0.49	0.49	0.70
G_{eff}	0.44	0.47	0.47	0.54	0.53	0.50
L_{eff}	0.96	0.94	0.93	0.89	0.89	0.92

TABLE VI. Network properties computed from the effective connectivity obtained in the different simulations performed in the striped network.

# Simulation	1	2	3	4	5	6	7
Rewiring (%)	0	0	0	0	0	0	10
n_{adj}	2	0	1	2	2	2	2
$h_{\uparrow}$	1	-	0.1	0.1	0.35	0.1	0.1
$h_{\downarrow}$	1	-	0.5	0.5	0.35	0.5	0.5
Damage BC (%)	-	-	-	-	-	5	-
Damage k (%)	-	-	-	-	-	5	-
a_L (mm)	1.45	1.68	1.44	1.52	1.51	1.43	1.63
δ	0.24	0.28	0.24	0.25	0.25	0.24	0.27
$\langle k \rangle$	236	70	199	205	198	137	162
Q	0.48	0.57	0.51	0.50	0.45	0.55	0.38
G_{eff}	0.55	0.43	0.54	0.53	0.53	0.51	0.53
L_{eff}	0.89	0.75	0.87	0.86	0.86	0.85	0.85

E. Impact of simulations' parameters on effective connectivity properties

The first aspect to note when studying the properties of the effective networks, *i.e.*, those obtained purely from the dynamics of the network, is that they vary greatly depending on the z–score chosen. For consistency with the rest of the results, we take $z = 1$ and study how the network properties vary for the different values of the parameters.

If we try to compare function to structure we see that very different values are obtained in the magnitudes for the same parameters, even in the case of maximum aggregation corresponding to the simulation #1 of the aggregated network, for which we obtain an effective adjacency matrix that almost equals the structural one, see FIG. 8(c,e,f). For all cases the average number of links $\langle k \rangle$ is much larger in the functional network and consequently a_L is also much larger in this case. By calculating the correlation lengths we observed that the average axonal length is much smaller than the characteristic length of the networks, indicating that strong spatial constraints somehow translated in perturbations in the communication between neurons. Thus, one could say that for strong spatial embedding, structure dictates functional behaviour.

If we look at the aggregated network we can clearly see that even the difference of values with the structural magnitudes, with 0% rewiring we obtain the most modular network, with smaller global efficiency and larger local efficiency. We also observe that, by increasing rewiring without damage, (#1-#5) Q and L_{eff} decrease, just as they did in the structural network. On the contrary, we obtain that the network with 20% rewiring has less global efficiency than the network with 13% rewiring.

In the case of the striped network it can also be identified that simulation #2 describes the most modular network, although it has the highest value of local efficiency instead of the lowest.

To see if the effective network captures structural prop-

erties, the distribution of angles formed by a connection with respect to the positive x–axis is calculated. The distribution is presented in FIG. 7. It is observed in the top two distributions that there is no privileged direction neither for the case of isolated modules (#1) nor after 6.5% rewiring (#3).

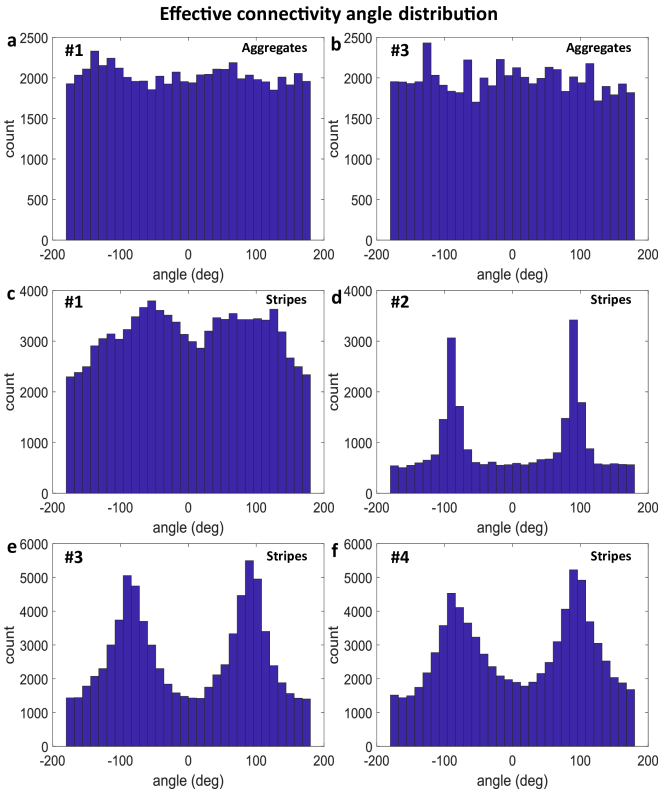

FIG. 7. Distribution of connectivity angles among pairs of effectively connected neurons. The top row correspond to the aggregated network, simulations #1 and #3. The two bottom rows correspond to the stripes network, simulations #1 to #4.

For stripes, we see that in the absence of stripes (#1) there is no privileged direction, although the distribution is not as smooth as in the case of aggregates. For the next three simulations (#2,#3,#4), two peaks at -90 and $+90$ degrees are clearly observed, indicating that the anisotropy imposed on the structural network imprints features on the effective network, with neuronal communication in the longitudinal direction (along stripes) being easier than in the transverse direction.

F. Detailed comparison of network behaviour — Aggregated network

Here we focus on studying some of the representative cases among the simulations done.

For the aggregated network we compare a simulation with isolated modules with a simulation with 6.5% rewiring, FIG. 8.

For 0% rewiring (FIG. 8a–f), as expected, the adjacency matrix is formed by a diagonal of boxes corresponding to the connections between the excitatory neurons of the different aggregates, with no other connections outside the diagonal (FIG. 8c). This is reflected in the raster plot, where the different modules fire independently about once every 10 seconds. The conversion of the raster plot to calcium concentration (FIG. 8d) allows comparison with experiments. In this case it is quite clean, being able to resolve the number of times any aggregate fires synchronously and at what time. Usually this is not possible in experiments, making it difficult to convert these data to raster plots. In any case, both in these simulations and in the experiments, it is practically impossible to resolve every single action potential.

The effective matrix calculated with TE reflects these results (FIG. 8e), as the inferred connectivity between modules due to noise and independent firing of neurons is minimal. To quantify these results, the structural and effective connectivity matrices are added together (FIG. 8f). The latter is previously multiplied by 4 such that the resulting matrix, S+E, contains a 0 for each element corresponding to connection absence in both the structural and the effective matrix, a 1 for each element present in the structural but not in the functional matrix, a 4 for each element present in the functional but not in the structural matrix and a 5 for each element present in both. The percentage of coincidence and the percentage of error (as presented in TABLE. IV) are calculated by comparing the results of the previous sum with the structural matrix. The first percentage is calculated from the ratio of the number of 5's in the S+E matrix to the total number of 1's in the structural matrix and the second percentage from the ratio of the number of 4's in the S+E matrix to the number of 0's in the structural matrix. In this case we obtain a coincidence percentage of 92.1% and an error percentage of 4.8%.

For the case where there is a 6.5% rewiring (FIG. 8g–l) we see that many connections have been formed just by looking at the network representation (FIG. 8g). These are far fewer than those present within the aggregates, as we can clearly observe in the structural connectivity matrix (FIG. 8i). In the raster plot, we observe a behaviour that combines local firing at module level with collective firing at the level of the whole network. In this case the conversion to a calcium signal is still very illustrative, but we can no longer discern when each module is firing. This is also seen in the effective connectivity matrix (FIG. 8k) where there are more off-diagonal connections than actually exist in the structural matrix . From the S+E matrix we obtain a coincidence percentage of 77.2% and an error percentage of 5.4%.

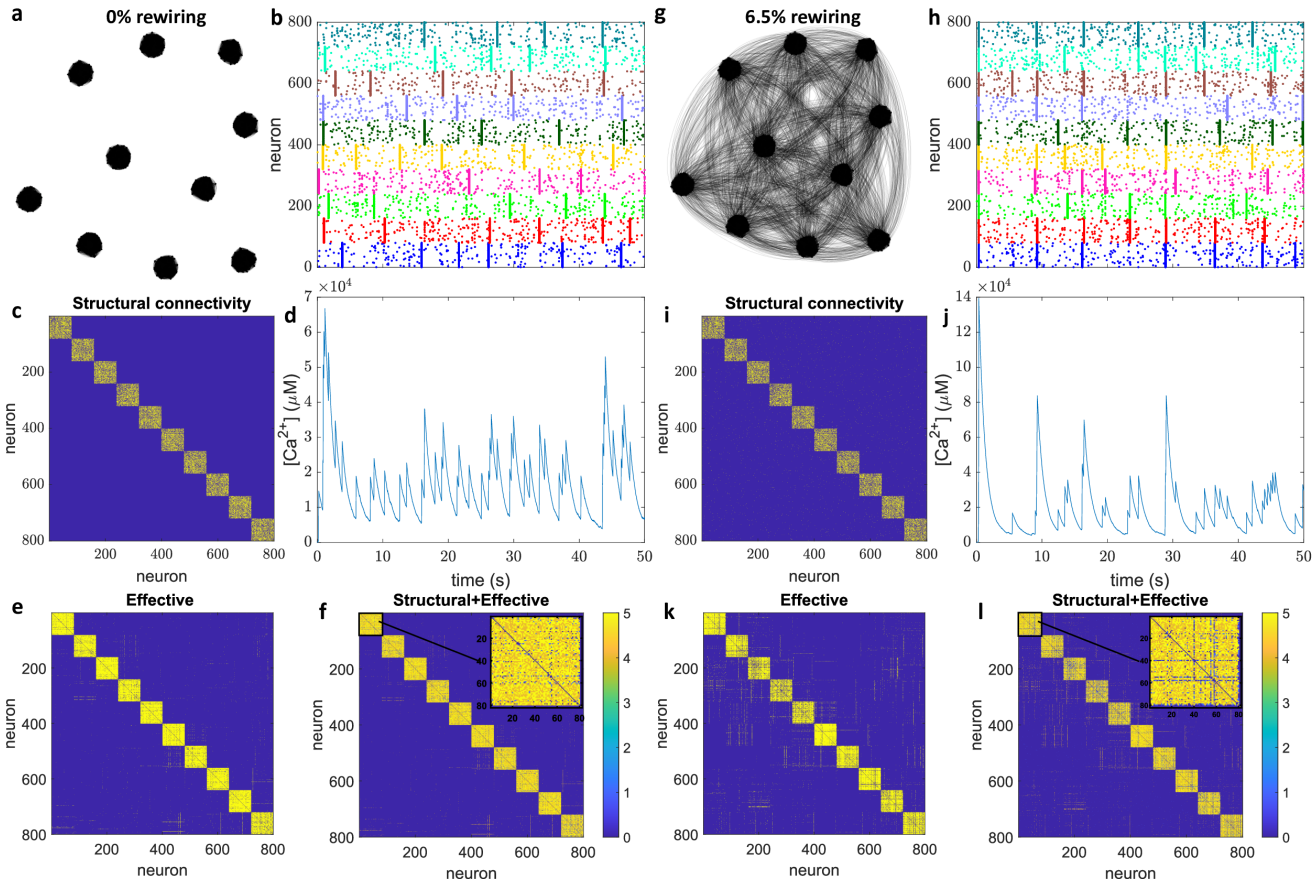

FIG. 8. **a-f**: 0% rewiring, **g-l**: 6.5% rewiring. Structural network representation from Gephi (**a**,**g**), structural connectivity matrix (**c**,**i**), effective connectivity matrix (**e**,**k**), raster plot (**b**,**h**), calcium concentration (**d**,**j**) and structural to effective comparison (**f**,**l**). The colours in the raster plots correspond to the different communities in FIG. 1.

G. Detailed comparison of network behaviour — Striped network

For the striped network we compare the homogeneous case (FIG. 9a-f) with the simulations with $h_\uparrow = 0.1$, $h_\downarrow = 0.5$ (FIG. 9g-l) and with $h_\uparrow = h_\downarrow = 0.35$ (FIG. 10). In all cases $n_{\text{adj}} = 2$.

For the homogeneous case, a highly connected matrix is obtained (FIG. 9a), as reflected by the average degree (TABLE. III) and bursting raster plot, with markedly synchronous activations (FIG. 9b,d). Still, the short length of the axons results in the formation of 9 clearly distinguishable communities in the structural connectivity matrix (FIG. 9c). These, however, are quite connected to each other. Still, as the axons are short, a large number of neurons are needed to pass information over long distances, resulting in low overall efficiency values ($G_{\text{eff}} = 0.66$ for the structural and $G_{\text{eff}} = 0.55$ for the effective). Although the effective matrix (FIG. 9e) captures quite well the different communities observed in the structural matrix, there are many connections that it does not infer correctly. Here the coincidence percentage is 75.2% and the error percentage amounts to 12.7%.

Both for the case with $h_\uparrow = 0.1$ and $h_\downarrow = 0.5$ and for the case with $h_\uparrow = h_\downarrow = 0.35$, we can observe that the stripes cause a strong restriction in the transverse direction. We can also observe that $h_\uparrow = 0.1$ and $h_\downarrow = 0.5$ lead to overall activity with weak bursting (FIG. 9h–j) whereas $h_\uparrow = h_\downarrow = 0.35$ lead to stronger bursting (FIG. 10b-d).

Thus, for this strongly connectivity–dictated network, there is a good balance between firing locally and globally, even though the axonal length is small. Of the communities detected in the structural connectivity matrix (FIG. 10c) there is one that is not recovered in the effective matrix (FIG. 10e). This is the simulation in which there is the least overlap between structure and function, with a 64.0% of coincidence percentage and an error percentage of 11.4%.

H. Impact of damage — Connectivity

We now study how the system changes when the system is damaged. As introduced in Methods, the 5% of nodes with the highest degree and the 5% of nodes with

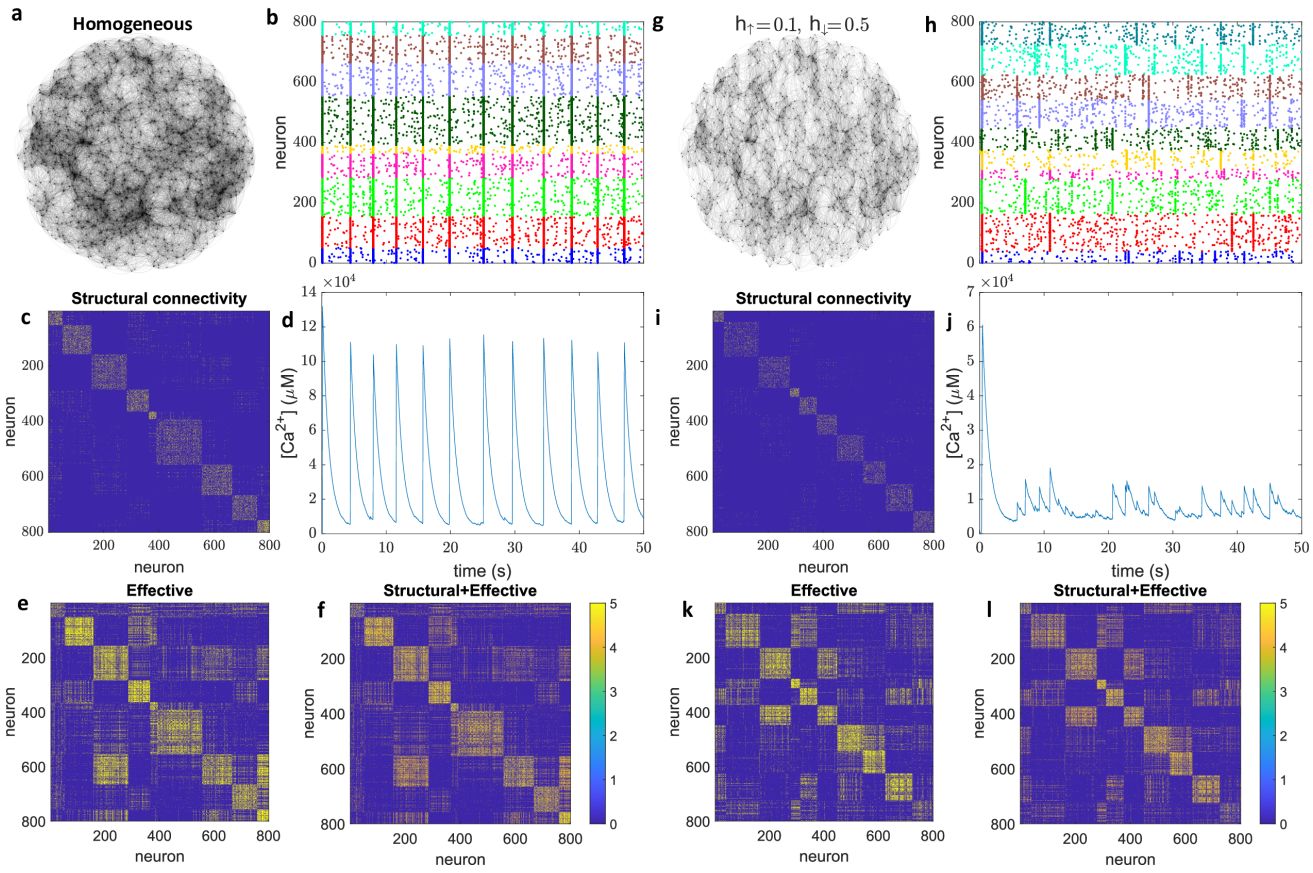

FIG. 9. **a-f**: 0% rewiring, $n_{\text{adj}} = 2$, $h_{\uparrow} = h_{\downarrow} = 1$; **g-l**: 0% rewiring, $n_{\text{adj}} = 2$, $h_{\uparrow} = 0.1$,$h_{\downarrow} = 0.5$. Structural network representation from Gephi (**a**,**g**), structural connectivity matrix (**c**,**i**), effective connectivity matrix (**e**,**k**), raster plot (**b**,**h**), calcium concentration (**d**,**j**) and structural to effective comparison (**f**,**l**).

the highest BC are eliminated for both the aggregated and the striped networks.

By comparing the network properties measured for both aggregated and striped networks without and with damage *i.e.*, simulations #3 and #6, TABLE. II, and simulations #4 and #6, TABLE. III, we do not see much difference. To make comparisons possible, we keep the same amount of rewiring constant and we keep the same parameters $h_{\uparrow,\downarrow}$ and number of adjacency stripes.

The most noticeable changes before and after the damage are the decrease in the average number of neighbours, $\langle k \rangle$, since multiple connections have been eliminated, and the slight reduction in local efficiency, more remarkable in the stripe network.

The comparison between undamaged and damaged effective networks show a greater difference than the comparison of structural networks just discussed. The changes in the calculated magnitudes can be due to both the removal of the neurons and respective connections and the specific dynamics of the simulations themselves.

To begin with, we study how the degree distributions and centrality coefficients change, as these are the elements that we change directly to damage the networks.

Figure FIG. 11 shows how the degree distribution of the structural and functional connectivity varies for both networks when they are damaged.

We see that, although in practice the number of connections is reduced, the average number of structural connections does not always decrease. An example is the case of the aggregated network whose network properties are extracted from the effective connectivity, (FIG. 11, top–right), as we have seen in TABLE. V. In the other three cases, we do observe a shift towards lower values of the mean value of connections, while maintaining the shape of the distribution. We observe that although the change is not very noticeable in the striped network computed from the structural connectivity, (FIG. 11, bottom–left), the effective connectivity network gets deteriorated a lot (FIG. 11, bottom–right), as many nodes are isolated or have very few connections. In this network there are a total of 99 neurons with a number of connections between $0 - 10$. In the striped network obtained from the effective connectivity there were 63 neurons with the same range of connections.

In FIG. 12 we study how varies the distribution in the betweenness centrality coefficients. We note that the centrality coefficients are normalised by the maximum value and, therefore, the distribution always refers to a neuron

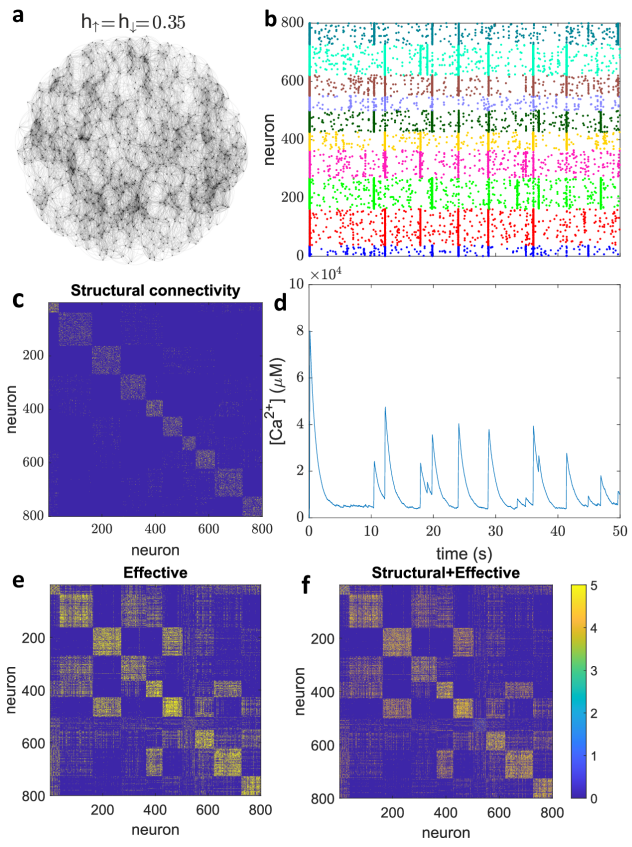

FIG. 10. **a-f**: 0% rewiring, $n_{\text{adj}} = 2$, $h_\uparrow = h_\downarrow = 0.35$. Structural network representation from Gephi (**a**), structural connectivity matrix (**c**), effective connectivity matrix (**e**), raster plot (**b**), calcium concentration (**d**) and structural to effective comparison (**f**).

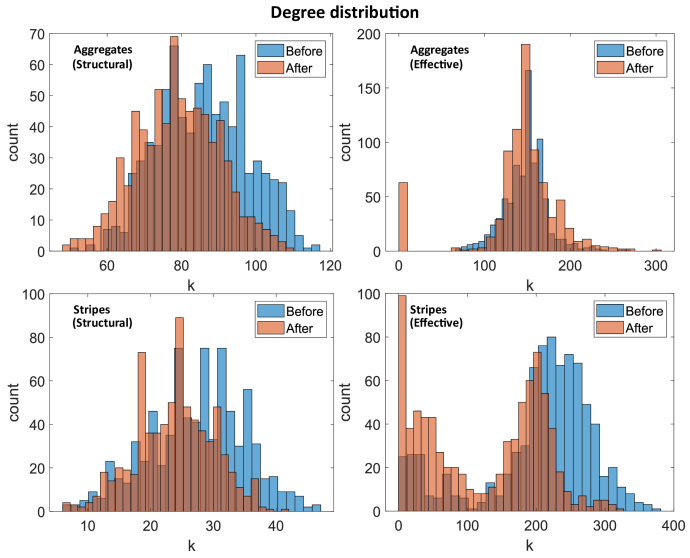

FIG. 11. Comparison of the degree distributions before and after damage. Representations on top correspond to the aggregated network and representations on bottom to the striped network. On the left computed from the structural connectivity on the right from the effective connectivity.

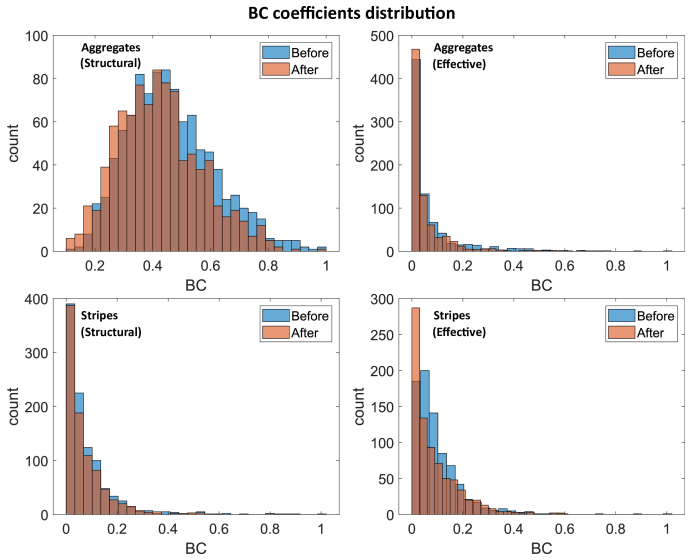

FIG. 12. Comparison of the BC coefficients before and after damage. Representations on top correspond to the aggregated network and representations on bottom to the striped network. On the left computed from the structural connectivity on the right from the effective connectivity.

with respect to that with the highest BC. Therefore, this makes it difficult to compare between different networks.

We limit ourselves to comment that qualitatively they all follow the same distribution before and after the damage. The one that looks most different from the others is the corresponding to the aggregated network obtained from structural connectivity, (FIG. 12, top–left). In this one, 75% of neurons have a normalised BC between 0.3 and 0.6 and quite a few above 0.6, while in the other distributions almost all neurons have a normalised BC below 0.2.

I. Impact of damage — Dynamics

We now focus on analysing how the dynamics change after the targeted attack. Since not much variation has been observed for the damage in the dynamics of the aggregated network, we only include below the comparison in the case of the striped network, FIG. 13, corresponding to simulations #4 (undamaged) and #6 (damaged).

At first glance (FIG. 13a–d), it can be seen that most of the eliminated connections belonged to the central region of the network. This is probably the reason why a lot of collective behaviour is observed to be lost (FIG. 13b–e). This can be quantified by means of the calcium concentration, because for the undamaged network the collective activation always exceeded calcium concentrations of 10 mM and for the damaged network this happens only twice (FIG. 13c–f), apart from the large collective firings due to the initial conditions. Note the change of scale on

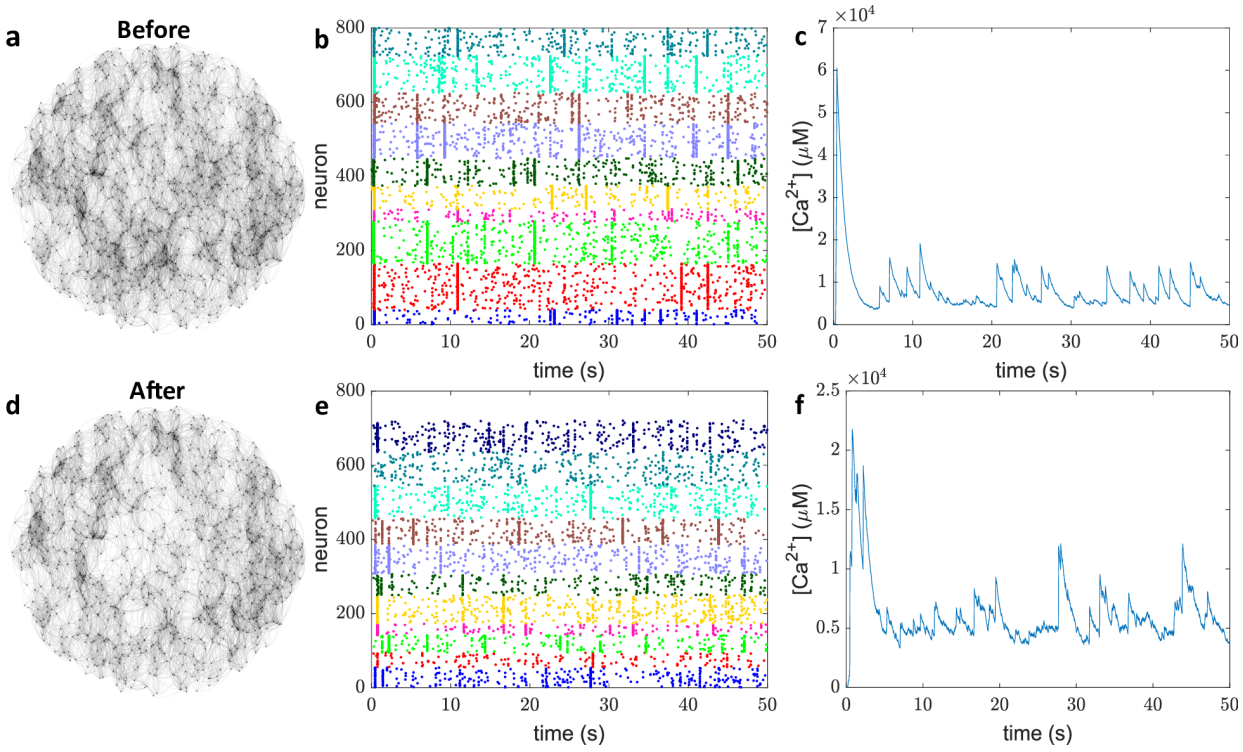

FIG. 13. Structural connectivity representation from Gephi (**a**,**d**), raster plot (**b**,**e**) and calcium concentration (**c**,**f**) for the network before damage (simulation #4, top) and after damage (simulation #6, bottom).

the ordinate axis between the two comparison plots.

The next step is to determine whether the deleted neurons —which *a priori* were among the most important at the level of degree and centrality— played an important role in the onset of the observed collective firings, that is, when more than 5% of the neurons fire. For this purpose, long simulations of 500 s were launched for both networks.

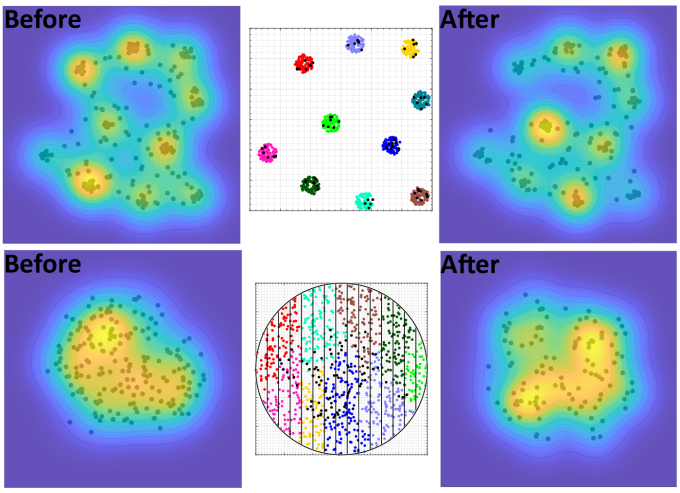

FIG. 14. Initiation points of activity before damage, damaged neurons and initiation points of activity after damage, for the aggregated network (top) and the striped network (bottom).

Figure FIG. 14 shows the activity initiation points of the collective firing before the damage, the deleted neurons (in black) and the initiation points after the damage. It is observed that in the case of damage to the aggregates, they continue firing in a similar way as they did before the damage, although the location of the initiation points varies when damage is received. Before the damage, 250 collective firings are recorded and after the damage, 248.

In the case of damage to the striped network, the activity decreases from 192 collective firings to 113, as can be seen in the lower representations of FIG. 13.

J. Comparison with experimental results with the stripes network

Finally, the results obtained from the striped network are compared with experimental results in FIG. 15. Specifically, the network fraction of neurons participating in the different collective firings is measured.

As in the experiment, we take as a control the network in stripe height absence, *i.e.*, the homogeneous case, simulation #1. To compare with this, 500 s simulations are simulated, first with $h_\uparrow = 0.1$ and $h_\downarrow = 0.5$ and then with $h_\uparrow = h_\downarrow = 0.35$. We find more similarity with the experiments for the latter case, having the same effective height $h_\uparrow = h_\downarrow = 0.35$ for both the high and low stripes.

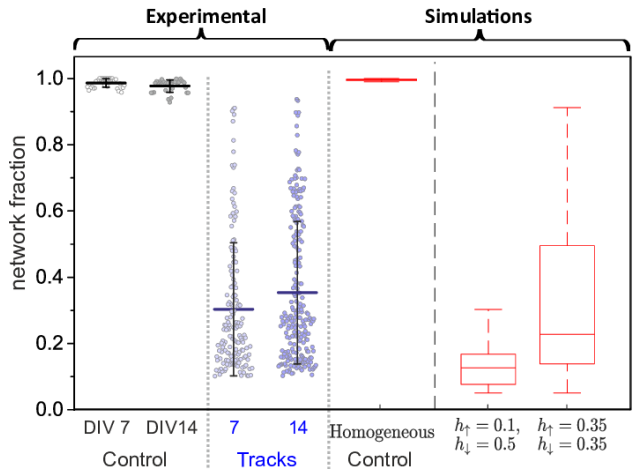

FIG. 15. Fraction of neurons firing in each collective firing. Comparison of the experimental results with the results obtained through numerical simulations. Outliers have been removed for clarity.

IV. DISCUSSION AND CONCLUSIONS

The numerical simulations presented here provide dynamics consistent with the experimental results reported in [6]. Specifically, for the aggregated network, 6.5% rewiring is sufficient to observe a balance between segregation and integration, *i.e.*, information processing at both local and global levels. In the striped network, this occurs for effective heights $h_\uparrow = h_\downarrow = 0.35$. Although in the experiments it is easier to connect from ridges to valleys than vice versa, here we see that these parameters are more optimal than $h_\uparrow = 0.1$ and $h_\downarrow = 0.5$. In the latter case the constraint may be too strong, so future work may include to study the variation of effective heights to exactly reproduce the experiments. The definition of how axons interact in the presence of level changes, as in [11], could also be improved.

It is worth noting the strong dependence both on the parameters we vary and on the model parameters themselves, such as the strength of the synapse connections or the characteristic decay time of the synaptic depression. Given the two imposed geometries, most of the parameters are fixed in order to observe how some others are varied.

Although the network properties calculated from structural connectivity reflect the network's inherent structure, it is complicated to compare these with the ones obtained from the effective network. This is because the choice of z-score is crucial as different thresholds lead to networks with a different number of effective connections. While an interesting alternative would be to stick with the strongest connections, corresponding to $z = 3$, $z = 1$ is set to have both weak and strong connections. This choice also corresponds to the case where the connectivity calculated by TE approaches with XC and MI.

As expected, the case in which we find the best match between the structural and effective matrices is, with a percentage of 92.1%, the aggregated network with independent modules. Even so, for the other cases we also manage to recover the communities and the connections between them, keeping a low percentage of error.

We have analysed the distribution in the angles formed by the axons from the effective connectivity, to see that while for the aggregated network the distribution is very homogeneous, the striped network preserves the strong spatial restriction in the transverse direction of the stripes.

We found the aggregated network to be very robust under a targeted attack. It is probably the high connectivity within the modules that makes the network resilient to attack on the hubs. An attack on nodes with more BC can be expected to disconnect the long distance connections created by rewiring, but as long as the percentage of damaged nodes is sufficiently lower than the number of connections between aggregates, global information exchange is possible. Let us note that with only 4% rewiring the network already reached a global efficiency $G_{\text{eff}} = 0.4$. On the contrary, the striped network becomes much weaker, losing many central connections and leads to a the decrease of activity.

ACKNOWLEDGMENTS

I would like to express my deepest gratitude to Jordi, for introducing me to the beautiful world of neuroscience and all the path we have followed to carry out this work. I would also like to offer my special thanks to Akke, who accompanied me on this the journey and has always been open to help me. Finally, I would like to thank my family and friends who are with me day after day.

[1] Alan L Hodgkin and Andrew F Huxley. A quantitative description of membrane current and its application to conduction and excitation in nerve. *The Journal of physiology*, 117(4):500, 1952.

[2] Hideaki Yamamoto, Satoshi Moriya, Katsuya Ide, Takeshi Hayakawa, Hisanao Akima, Shigeo Sato, Shigeru Kubota, Takashi Tanii, Michio Niwano, Sara Teller, et al. Impact of modular organization on dynamical richness in cortical networks. *Science advances*, 4(11):eaau4914, 2018.

[3] Eugene M Izhikevich. Simple model of spiking neurons. *IEEE Transactions on neural networks*, 14(6):1569–1572, 2003.

[4] Sara Teller, Clara Granell, Manlio De Domenico, Jordi Soriano, Sergio Gómez, and Alex Arenas. Emergence of assortative mixing between clusters of cultured neurons.

PLoS computational biology, 10(9):e1003796, 2014.

[5] Elisenda Tibau, Adriaan-Alexander Ludl, Sten Rüdiger, Javier G Orlandi, and Jordi Soriano. Neuronal spatial arrangement shapes effective connectivity traits of in vitro cortical networks. *IEEE Transactions on Network Science and Engineering*, 7(1):435–448, 2018.

[6] Marc Montalà-Flaquer, Clara F López-León, Daniel Tornero, Tanguy Fardet, Pascal Monceau, Samuel Bottani, and Jordi Soriano. Rich dynamics and functional organization on topographically designed neuronal networks in vitro. *Available at SSRN 4111611*.

[7] Olav Stetter, Demian Battaglia, Jordi Soriano, and Theo Geisel. Model-free reconstruction of excitatory neuronal connectivity from calcium imaging signals. 2012.

[8] Mark EJ Newman. Modularity and community structure in networks. *Proceedings of the national academy of sciences*, 103(23):8577–8582, 2006.

[9] Joshua T Vogelstein, Brendon O Watson, Adam M Packer, Rafael Yuste, Bruno Jedynak, and Liam Paninski. Spike inference from calcium imaging using sequential monte carlo methods. *Biophysical journal*, 97(2):636–655, 2009.

[10] Sergio Faci-Lázaro, Jordi Soriano, and Jesús Gómez-Gardeñes. Impact of targeted attack on the spontaneous activity in spatial and biologically-inspired neuronal networks. *Chaos: An Interdisciplinary Journal of Nonlinear Science*, 29(8):083126, 2019.

[11] Adriaan-Alexander Ludl and Jordi Soriano. Impact of physical obstacles on the structural and effective connectivity of in silico neuronal circuits. *Frontiers in computational neuroscience*, 14:77, 2020.